Eksploatacja i Niezawodnosc - Maintenance and Reliability
Volume 29 (2027), Issue 1
https://ein.org.pl

The Polish Maintenance Society

Intelligent control method for continuous miner cutting parameters based on strength constraints

Xunan Liu[1,2], Yongqiang Dong[1,*], Jianzhuo Zhang[1], Yadong Wang[1], Lijuan Zhao[1,2]

[1] School of Mechanical Engineering, Liaoning Technical University, Fuxin 123000, China
[2] State Key Lab of mining machinery engineering of coal industry, Liaoning Technical University, Fuxin 123000, China
* Corresponding Author: 2422034330@qq.com

Received: 9 May 2026
Revised: 10 May 2026
Accepted: 1 June 2026
Online: 17 July 2026

Abstract

To address the issues of insufficient dynamic strength and low energy efficiency in continuous miners operating in complex coal seams, this paper investigates the dynamic characteristics and intelligent control of the EML340 continuous miner. A rigid-flexible coupled virtual prototype was developed, revealing that the stress at the cutting arm's hydraulic cylinder connection exceeds the allowable limit (125 MPa) under baseline conditions. Single-factor analysis and response surface methodology were employed to quantify the individual and interactive effects of drum speed, swing speed, and coal-rock hardness on peak stress and specific cutting energy (SCE), with local sensitivity further identifying swing speed as the most influential factor on stress. Based on these analyses, an intelligent Fuzzy Neural Network (FNN) controller was designed, incorporating a three-level parallel safety protection module. Co-simulation using ADAMS and MATLAB/Simulink demonstrates that the FNN controller adaptively adjusts rotational and swing speeds in response to hardness variations. Ablation experiments confirm that the integrated FNN architecture outperforms pure fuzzy control and pure BP neural network in settling time, overshoot, steady-state error, and safety constraint satisfaction. Robustness analysis verifies stable operation even under ±50% internal parameter perturbations. The simulation accuracy was validated via a physical cutting test bench, showing a maximum relative error of 4.92% in vibration characteristics, and variable-hardness cutting experiments further confirm the controller's adaptive regulation performance. This research provides a theoretical basis and technical solution for achieving intelligent, efficient, and safe cutting in continuous miners.

Keywords: *miner, cutting system, dynamic strength, fuzzy neural network, intelligent control*

Article citation:
Liu X, Dong Y, Zhang J, Wang Y, Zhao L, Intelligent control method for continuous miner cutting parameters based on strength constraints, Eksploatacja i Niezawodnosc – Maintenance and Reliability 2027: 29(1) http://doi.org/10.17531/ein/223922

Highlights

- Rigid-flexible coupling model reveals stress hazard in continuous miner cutting arm.
- FNN controller adapts drum speed and swing speed to coal-rock hardness variations.
- FNN control reduces overshoot by 28.6% and settling time by 87.5% versus PID.
- Cutting energy reduced by 9.3% while ensuring peak stress stays below 125 MPa limit.

1. Introduction

The Continuous Miner (CM) is primarily used for coal extraction in room and pillar mining and can also be employed for roadway development. It is a large-scale, continuous excavation machine integrating cutting, loading, and transportation functions, suitable for mining coal seams ranging from 1.5 to 6 meters in thickness. Due to complex geological conditions, the cutting unit of the CM is subjected to severe alternating loads when cutting hard coal seams. Prolonged operation under these conditions frequently leads to cracks or even fractures in the cutting arm housing. Statistics indicate that such failures account for 30% of all CM failures [1]. Furthermore, the highly variable nature of coal and rock properties leads to nonlinear fluctuations in cutting loads, making it difficult to establish a reliable mapping relationship between the SCE and coal-rock properties [2]. This results in machine overload when cutting hard coal sections and energy waste when cutting soft coal sections. These issues not only threaten mining safety, shorten equipment service life, and increase maintenance costs, thereby constraining energy efficiency and impacting overall production economics. In response, researchers have conducted extensive studies on the strength reliability of mining machinery, SCE, and intelligent control.

In research on the reliability of mining equipment, Li Ruzhi [3] addressed the frequent breakage of connecting bolts in the rocker arm of the MG500/1220-WD shearer by implementing a reinforced design that increased the number of bolts and improved material quality. Zhang Xiao et al. [4] used finite element software to simulate the fatigue life of a planetary carrier, identifying stress concentration areas. With advancements in computer technology, combined multi-body dynamics and finite element analysis methods have been widely adopted: Lei Xianqiang et al. [5] established a rigid-flexible coupled virtual prototype of the cutting unit to analyze stress and deformation in key components. Zhao Lijuan et al. [6] conducted dynamic and fatigue analysis on transmission system gears but did not account for system coupling effects. Liu Shuhua [7] improved simulation accuracy by modeling in ADAMS and simulating loads using Matlab. Liu Xiao [8] used Pro/E and ANSYS Workbench for finite element analysis of different relief groove structures to determine the optimal mechanical design. Additionally, Wang Guang [9] analyzed pin strength through co-simulation and established a load-strength interference model. Liu Xunan [10] performed strength analysis and life prediction for key components based on reliability theory.

SCE (SCE) is a crucial indicator for evaluating the cutting efficiency of mining machinery. Liao Jiubo et al. [11] investigated the effects of different cutting depths and pick line spacings on the cutting force and SCE of conical picks through laboratory linear cutting tests, providing a basis for pick arrangement optimization. Ji Mingtao [12] used PFC finite element software to analyze the influence of different pick installation angles on drum force and SCE, determining 45° as the optimal angle. Zhang Hongqing et al. [13] established a mathematical model and objective function with the motion parameters of the roadheader's cutting unit as design variables, using the linear weighting method, resulting in improved comprehensive cutting performance. Chi Nan [14] analyzed the influence of coal seam dip angle, swing speed, and cutting depth on SCE, finding swing speed to have the most significant effect. Wu Qiong [15] used discrete element simulation to study the impact of swing speed and cutting speed on performance, achieving enhanced efficiency and reduced energy consumption. Zhang Yanpeng studied the influence of CM drum motion parameters on drum cutting power, cutting arm energy consumption, cutting fluctuation coefficient, and cutting area.

In the field of intelligent control, J. Świder and D. Jasiulek [16] developed a .NET-based simulation program and constructed a virtual prototype for a roadheader control system. Yan Luchao [17] established an adaptive control model for the hydraulic system using an improved particle swarm optimization algorithm, verifying its robustness. Zhao Lijuan and Li Miao [18] combined a fuzzy controller with PID to enhance the speed and anti-interference capability of the height adjustment system. Chen Jinguo et al. [19] established a mathematical model for the height adjustment system and adopted a fuzzy adaptive PID controller, demonstrating the superiority of closed-loop control. Wang Hui et al. [20] proposed a fuzzy PID control with parameter self-tuning based on the univariate marginal distribution algorithm, strengthening the system's anti-interference ability. Mao Jun and Guo Hao [21] proposed a novel firefly algorithm to optimize the PID strategy. Liu Litao and Dong Shutang [22] implemented adaptive cutting speed regulation using a BP neural network. Guo Dong et al. [23] established a TBM tunneling parameter prediction model based on deep learning. Zhao Lijuan et al. [24] constructed an integrated mechanical-electrical-hydraulic-control adaptive cutting system. Liu Chunsheng et al. [25] proposed a binary cooperative control mode combining autonomous height adjustment and speed regulation. Cai Anjiang et al. [26] built an implicit digital twin model and optimized trajectory prediction using the honey badger algorithm. Zheng Chuang et al. [27] proposed a process-driven intelligent cutting control scheme, achieving adaptive coupling and automatic height adjustment. Liu Songyong et al. [28] designed an automatic height control system that uses radar to identify the coal-rock interface and employs an indirect adaptive control method based on a neural network observer to achieve trajectory tracking and performance optimization.

In summary, while existing research has made significant progress in various aspects, it often focuses on static strength analysis or single control strategies. There is a lack of research that deeply integrates the dynamic stress response of key components with holistic intelligent control strategies, making it difficult to achieve the synergistic optimization of safety and energy efficiency. This study focuses on the EML340 continuous miner and systematically conducts research on the dynamic strength analysis of key cutting unit components under complex working conditions and intelligent control strategies. By constructing a multi-objective optimization model that incorporates dynamic stress constraints, it aims to achieve intelligent, efficient, and low-energy cutting, while ensuring the safety of key components. This work provides a theoretical basis and technical support for enhancing the comprehensive performance of continuous miners in complex coal seams.

2. Kinematic analysis of the cutting system

2.1. Operating principle of the continuous miner

The continuous miner is a comprehensive mining equipment that integrates the functions of roadway driving and short-wall mining, making it widely suitable for the extraction of coal seams with varying thicknesses. The basic operational process of the EML340 continuous miner comprises two key steps: "undercutting" and "pillar splitting," as illustrated in Figure 1. As the more time-consuming phase with a more significant impact on both safety and resource recovery rate, the "pillar splitting" step directly constrains the overall mining efficiency and economic benefits.

2.2. Analysis of drum load and SCE

(1) Drum Load Analysis

Based on classical pick force and coal fragmentation theory, a calculation program was developed in MATLAB to determine the three-directional forces and moments on the drum according to load calculation formulas [29]. By inputting different working condition parameters, the program directly outputs theoretical values of the instantaneous drum loads and generates curves of the instantaneous three-directional forces and moments acting at the drum's center of mass. The resulting curves of the three-directional forces and moments on the drum are shown in Figure 2. The labels Rx, Ry, Rz represent the three-directional forces, and Mx, My, Mz represent the three-directional torques. Specifically, Rx denotes the cutting resistance, Ry denotes the traction resistance, and Rz denotes the axial force. Mx, My, and Mz are the corresponding torques about the X, Y, and Z axes, respectively.

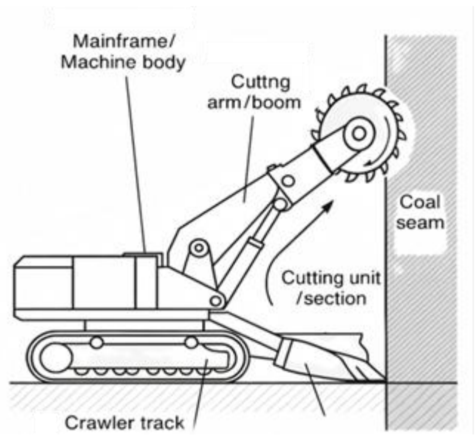

Figure 1. Schematic diagram of the continuous miner.

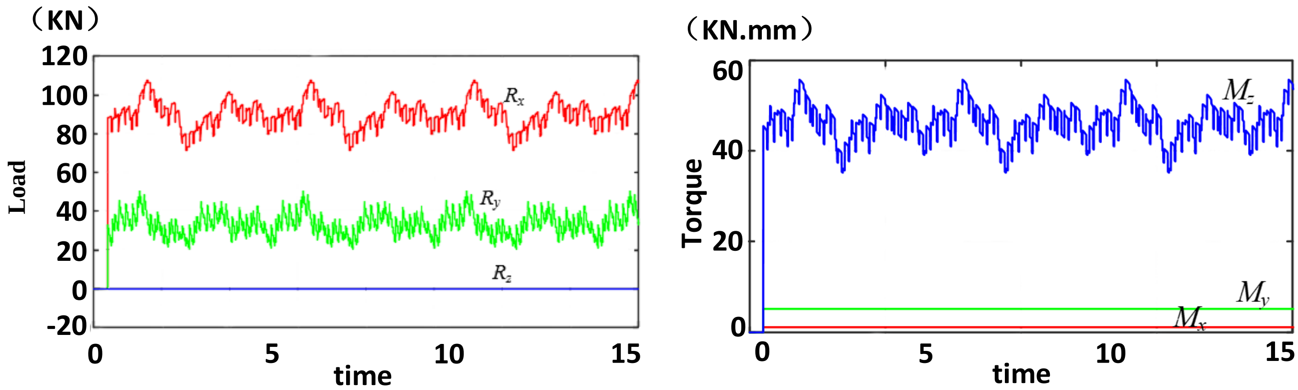

Figure 2. Load curve.

(2) Specific Cutting Energy Analysis

Specific cutting energy (SCE) is a key indicator for evaluating the cutting efficiency of continuous miners, defined as the energy consumed per unit volume of fragmented coal or rock. The SCE (H_w) is influenced by the coupled effects of multiple parameters, including drum speed, swing speed, and coal-rock properties. It is calculated using the following formula:

$$H_w = \frac{P_M}{60 \cdot h_g \cdot h_c \cdot v} \tag{1}$$

where H_w denotes the specific cutting energy (kW·h/m³), P_M is the power consumed by the cutting head (kW), h_g is the drum cutting height (m), h_c is the drum cutting depth (m), and v is the linear velocity of the cutting mechanism (m/min).

The power consumption of the cutting head can be expressed as:

$$P_M = \frac{M_g \times n}{9550} \tag{2}$$

where: M_g is the total resistance torque, in N·m; n is the rotational speed of the cutting head, in r/min.

3. Model construction of the continuous miner cutting system

3.1. SolidWorks-based solid model construction

Based on the actual parameters of the EML340 continuous miner, a three-dimensional model of the cutting unit was developed in SolidWorks. This model encompasses core components such as the cutting arm, hydraulic system, and drum, as shown in Figure 3. It serves as the geometric foundation for subsequent dynamic simulations.

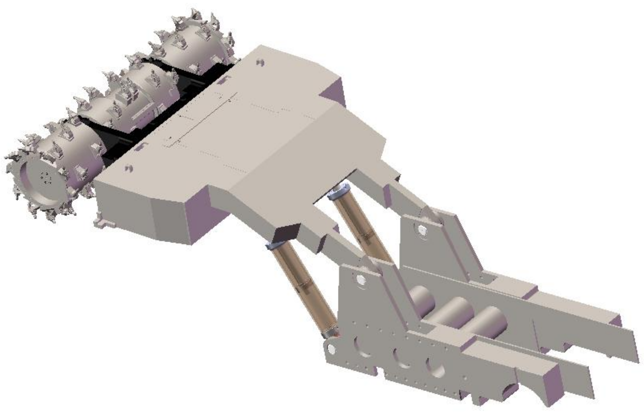

Figure 3. Overall model of the cutting section.

3.2. Development of a rigid-flexible coupled model in ADAMS

(1) Model Import and Material Definition

The 3D model of the cutting unit was imported into ADAMS in x_t format, followed by the definition of material properties. Standard materials (e.g., 45 steel) were assigned parameters directly from the software's built-in database. For special materials such as ZG310-570, a custom material was created manually with the following parameters: Young's modulus of 2.10×10^5 MPa, density of 7.82×10^3 kg/m³, Poisson's ratio of 0.293, and an allowable stress of 125 MPa.

(2) Generation of the Flexible Cutting Arm Body

To accurately capture the stress state of the cutting arm, a flexible body representation was created for it within ANSYS. First, the material properties of the cutting arm were defined. External connection points, or interface nodes, were established at critical joint locations. These included: The connection to the main frame (for defining a revolute joint). The connection to the hydraulic cylinder (for transmitting hydraulic forces). The connection to the drum (featuring 3 interface points to ensure proper load transfer). The model was meshed using SOLID45 elements, culminating in the generation of a Modal Neutral File (MNF), as illustrated in Figure 4.

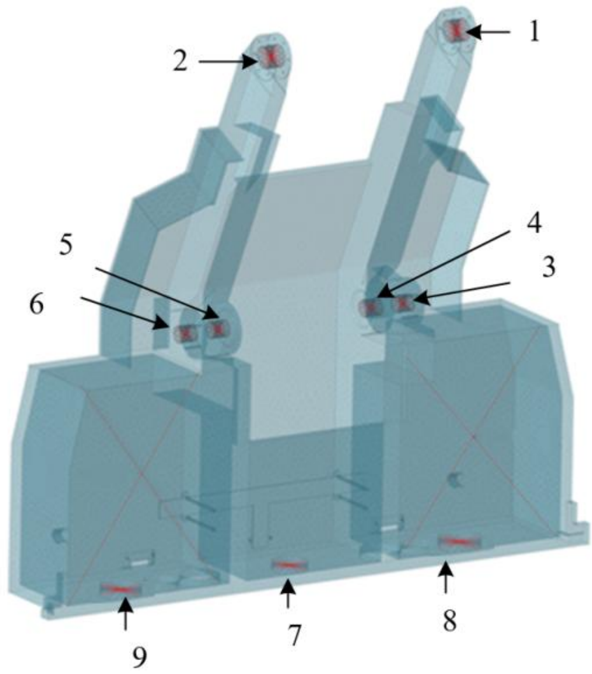

Figure 4. Modal neutral file of the cutting arm.

The MNF file was imported into ADAMS to replace the rigid cutting arm. Subsequently, its connection constraints with other components were re-established to ensure proper load transfer and motion coordination.

(3) Constraints and Motions

To ensure the correct relative positions between components, necessary constraints and motion excitations were applied. The constraints were defined as follows: a fixed joint was established between the main frame and the ground; revolute joints were added between the hydraulic cylinder and the cutting arm, as well as between the cylinder and the main frame; a translational joint was defined between the piston rod and the cylinder barrel; and a revolute joint was created between the drum and the cutting arm. For motion definition, an angular velocity excitation, STEP(time, 0, 0, 0.1, 246d), was applied to the drum's revolute joint, accelerating the drum to approximately 41 r/min within 0.1 seconds. A translational drive, STEP(time, 0, 0, 0.1, 34.285), was applied to the hydraulic cylinder's translational joint, enabling the cutting arm to achieve a swing speed of 7 m/min in 0.1 seconds. The mapping between cylinder speed and arm swing speed is approximately linear within the operational range (R^2 = 0.9986, σ = 0.342 mm/s), validating the use of a linear gain model for control design.

(4) Load Application

The three-directional forces and moments calculated in Section 2.3 were imported into ADAMS in the form of spline curves. A generalized force/moment element was created at the center of mass of the drum, with the spline data assigned as time-varying amplitudes. This approach enabled the accurate application of dynamic cutting loads.

(5) Establishment of the Rigid-Flexible Coupled Cutting System Model

The rigid-flexible coupled model of the cutting system is shown in Figure 5. Verification confirmed that the system's degrees of freedom were properly configured, with coordinated motion achieved (i.e., the hydraulic cylinder successfully drove the swing of the cutting arm, and no abnormal reaction forces were observed at the drum). The dynamic simulation was then initiated with a duration of 4 seconds and a step size of 0.004 seconds, employing the GSTIFF integrator and the SI2 equation formulation.

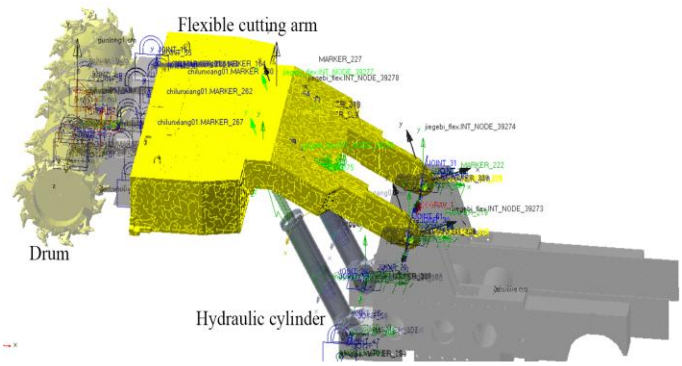

Figure 5. Rigid-flexible coupling model of the continuous miner.

3.3. Simulation results

(1) System Motion State Verification

Upon completion of the simulation, the time-domain curves of the hydraulic cylinder's extension/retraction speed and the cutting arm's swing angle were analyzed to verify whether the system's motion state aligned with the preset parameters.

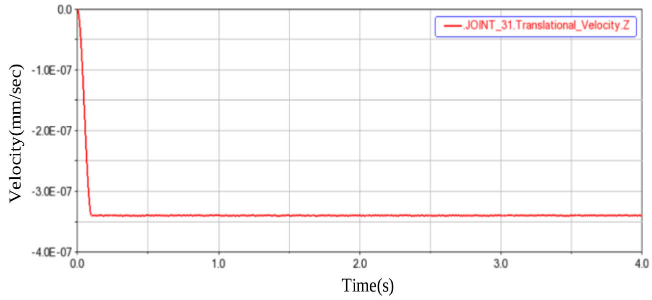

Figure 6. The extension speed curve of the hydraulic cylinder.

As shown in Figure 6, the hydraulic cylinder's extension/retraction speed stabilizes around the setpoint of 34.29 mm/s, with fluctuations remaining within the permissible error range. This indicates stable and smooth operation of the hydraulic drive system.

(2) Stress Distribution Analysis of the Cutting Arm

The "Hot Spot Analysis" function within the ADAMS/Durability module was utilized to identify critical stress zones from the simulation results. With the stress threshold set at 100 MPa, all nodal points were scanned throughout the entire simulation cycle. The results were compiled into a hot spot statistics table (Table 1), ranked in descending order of maximum stress.

Table 1. Identification of stress hotspots in the cutting arm.

Node ID	Location	Max Stress (MPa)	Time of Occurrence (s)	Remarks
198	Hydraulic Cylinder Connection	128.93	0.12	Exceeds allowable stress (125 MPa)
342	Hydraulic Cylinder Lug	119.46	0.13	Within allowable stress range
127	Mid-section of Cutting Arm	108.72	0.15	Within allowable stress range
485	Gearbox Connection	92.58	0.18	Within allowable stress range
246	Upper End Cover	85.36	0.22	Within allowable stress range

Under the baseline operating condition (f = 3, n = 41 r/min, v = 7 m/min), Node 198, located at the hydraulic cylinder connection pin hole, reached a peak stress of 128.93 MPa at t = 0.12 s. This value exceeds the material's allowable stress, indicating a risk of strength failure. The stress contour plot (Figure 7) further reveals that high-stress regions are concentrated around the hydraulic cylinder connection area, which is consistent with the findings from the hot spot analysis.

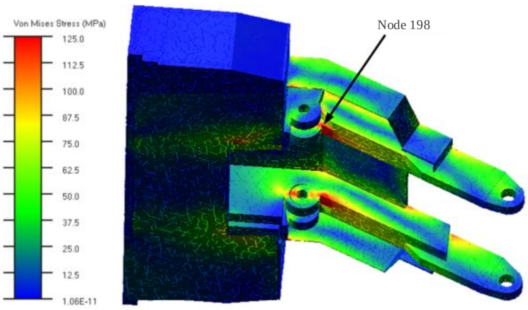

Figure 7. Stress contour plot of the cutting arm.

The stress time-history curve of Node 198 (Figure 8) indicates that the stress rapidly rises to its peak during the initial loading phase, followed by sustained high-frequency oscillations. The frequency of these oscillations corresponds to the periodic cutting load induced by the drum rotation speed (41 r/min). Such high-amplitude fluctuations will significantly impact the fatigue life of the cutting arm. Therefore, structural optimization or improved control strategies are required to mitigate the dynamic stress level.

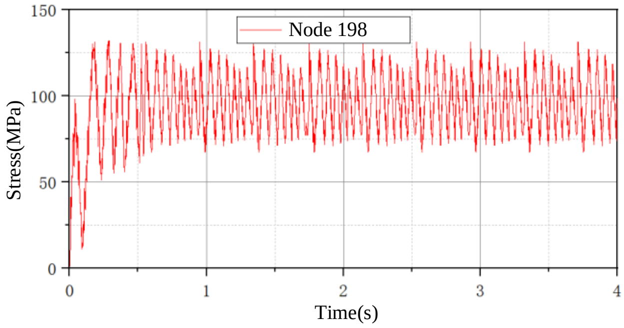

Figure 8. Stress curve of node 198.

4. Influencing factors and identification method

4.1. Univariate analysis

A single-factor analysis was conducted to investigate the effects of drum speed (n), swing speed (v), and coal-rock hardness coefficient (f) on cutting arm stress. Figure 9 shows the results under baseline conditions (v = 6 m/min, f = 3 for n variation; n = 31 r/min, f = 3 for v variation; n = 31 r/min, v = 6 m/min for f variation).

As n increases from 31 to 71 r/min, the maximum stress decreases by 3.88% (from 128.93 to 123.93 MPa), as higher rotational speed reduces cutting thickness per pick and mitigates impact loads. Conversely, as v increases from 3 to 7 m/min, stress rises by 9.45% (from 121.78 to 133.29 MPa) due to increased material removal volume per unit time and enhanced dynamic effects. The hardness coefficient f exhibits a nonlinear positive correlation with stress, with a pronounced acceleration when $f > 2.0$, attributed to the rapid increase in cutting resistance. These results indicate that swing speed is the most sensitive operational parameter affecting structural stress, while drum speed offers limited stress reduction at the cost of energy efficiency and pick wear. Appropriate parameter adjustment based on coal-rock hardness is therefore essential for balancing safety and productivity.

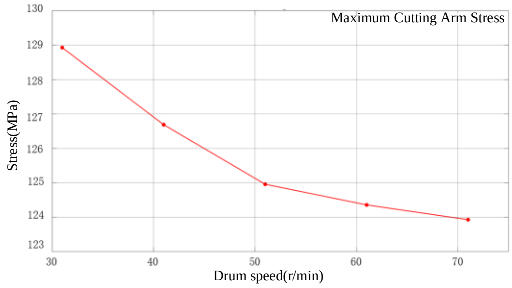

(a)

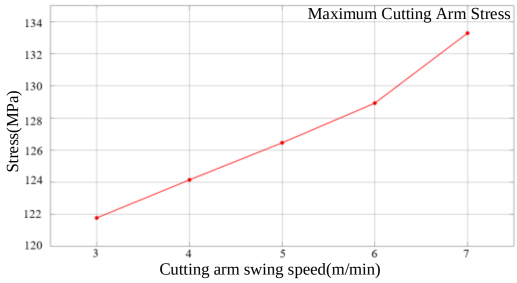

(b)

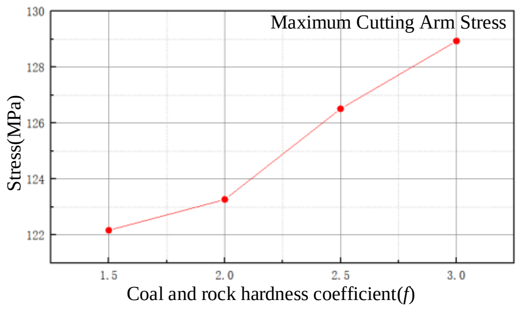

(c)

Figure 9. Effects of key parameters on cutting arm stress.

4.2. Response surface analysis

Based on the univariate experiments, to investigate the interactive effects and optimize the three factors-coal rock firmness coefficient (f), cutting arm swing speed (v), and drum rotation speed (n)-on the maximum stress (σ) of the continuous miner cutting head and the SCE (Hw), a response surface analysis was conducted using the Box-Behnken design (BBD).

(1) Experimental Design

Based on the results of the univariate experiments, the levels of each factor are shown in Table 2.

Table 2. Factors and levels for response surface analysis.

Factors	Low level	Center point	High level
Firmness coefficient (*f*)	1.5	2.5	3.0
Cutting arm swing speed *V*(m/min)	3	5	7
Drum rotation speed *n*(r/min)	31	51	71

A total of 15 experimental points were designed, of which 12 were factorial points and 3 were center point replicates used to estimate the pure error. The experimental design and results are shown in Table 3.

Table 3. Response surface experimental design and results.

	f	*V*	*n*	Maximum	*SCE* H_w
1	1.5	3	51	122.2	18.24
2	3.0	3	51	127.5	15.03
……	……	……	……	……	……
……	……	……	……	……	……
……	……	……	……	……	……
15	2.5	5	51	126.5	10.66

(2) Response Surface Model Establishment

A quadratic polynomial was used to perform regression fitting on the experimental data. The model forms are as follows:

Maximum stress σ model:

$$\begin{aligned} r = 126.50 + 2.25X_1 + 2.80X_2 - 2.60X_3 \\ +0.80X_1^2 - 0.50X_2^2 + 0.20X_3^2 \\ +0.60X_1X_2 - 0.40X_1X_3 + 0.30X_2X_3 \end{aligned} \tag{3}$$

The coefficient of determination R^2=0.976, and the adjusted R^2_{adj} = 0.954, indicating a good model fit.

Figure 10. Response surface and contour plots for maximum stress *σ*. *f* and *v* exhibit a positive interaction: when both increase simultaneously, *σ* increases significantly, indicating that high-strength coal rock combined with a high swing speed sharply increases the force on the cutting pick. *f* and *n* exhibit a negative interaction: increasing the drum rotation speed can, to some extent, alleviate the stress concentration caused by a high *f*. The interaction between *v* and *n* is weak, with contour lines nearly parallel, indicating that the two factors can be approximately regarded as having independent effects.

Specific cutting energy consumption H_w model:

$$\begin{aligned} \partial_w = 10.66 - 1.25X_1 - 3.40X_2 + 4.10X_3 \\ + 0.50X_1^2 + 1.20X_2^2 - 0.80X_3^2 \\ - 0.30X_1X_2 + 1.80X_1X_3 - 1.50X_2X_3 \end{aligned} \tag{4}$$

The coefficient of determination R^2=0.983, and the adjusted R^2_{adj} = 0.952, indicating high fitting accuracy.

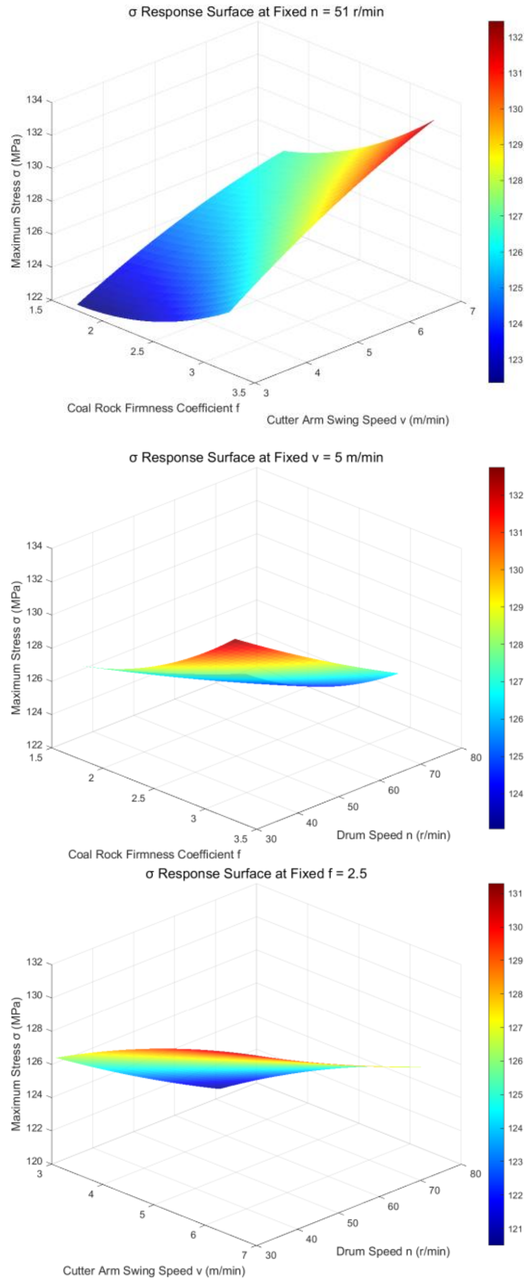

Figure 10. Response surface and contour plots for maximum stress.

As shown in Figure 11, *f* and *n* exhibit a strong positive interaction: at high rotation speeds, the amplifying effect of f on H_w is more pronounced, indicating that hard coal rock combined with a high rotation speed significantly increases the energy consumption per unit volume. *v* and *n* exhibit a negative interaction: increasing the swing speed can effectively suppress the increase in energy consumption caused by high rotation speeds, reflecting a "dilution" effect of high swing speed on energy consumption. The interaction between *f* and *v* is not significant, and their effects on energy consumption are relatively independent.

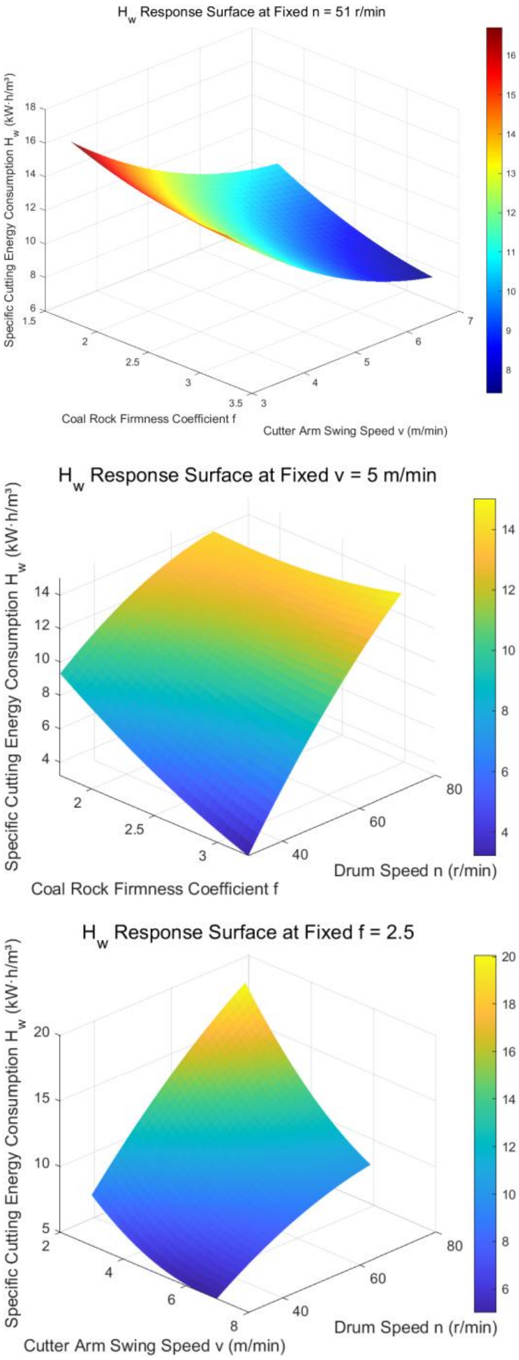

Figure 11. Response surface and contour plots for SCE.

4.3. Local sensitivity

Figure 12 shows the local sensitivity (absolute value of partial derivative) of each factor to maximum stress σ and specific energy consumption Hw at the center point. For maximum stress σ, swing speed v exhibits the highest sensitivity (2.80), followed by coal-rock firmness coefficient *f* (2.25), while drum rotation speed n shows the lowest sensitivity (2.60, with a negative sign). This indicates that the most effective way to control peak stress on the pick is to adjust the swing speed, followed by adapting to coal-rock conditions, while the effect of rotation speed adjustment is limited. In practice, when stress exceeds the limit, the swing speed should be reduced first.

For specific energy consumption Hw, drum rotation speed n exhibits the highest sensitivity (4.10), followed by swing speed *v* (3.40), while coal-rock firmness coefficient f shows the lowest sensitivity (1.25). This indicates that to reduce specific energy consumption, priority should be given to optimizing the drum rotation speed, followed by matching a reasonable swing speed. Although a high rotation speed can reduce peak stress, it significantly increases specific energy consumption, so a balance between the two must be sought. Moreover, the low sensitivity of *f* suggests that changes in coal-rock hardness within a certain range have a less significant effect on specific energy consumption than operational parameters.

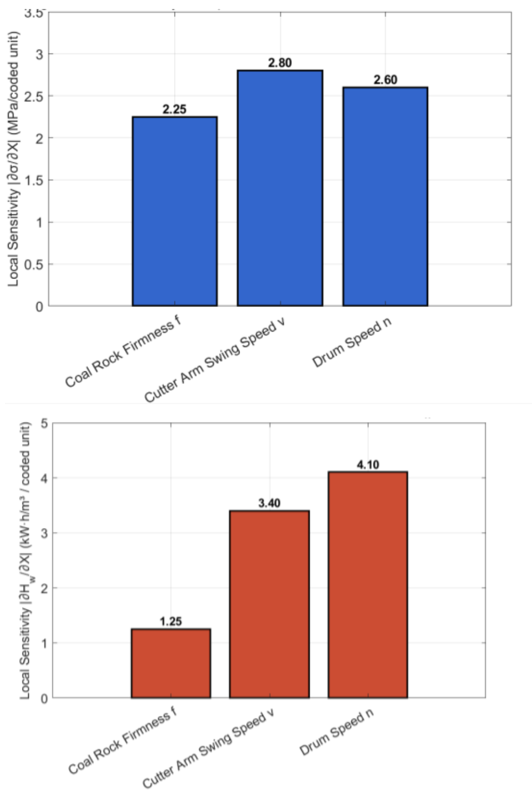

Figure 12. Local sensitivity of factors to σ and *Hw*.

4.4. Online identification method for coal rock firmness coefficient

In practical engineering applications, the coal rock firmness coefficient f cannot be measured directly. To address this, this paper adopts a coal rock identification method previously developed by our research group, which is based on cutting vibration response [30]. As shown in Figure 23, triaxial vibration acceleration sensors are installed on the cutting arm and drum bearing housing of the continuous miner to collect real-time vibration time-domain signals in the cutting resistance direction. A data-adaptive weighted fusion algorithm is then used to fuse the multi-source signals. Continuous wavelet transform is applied to convert the one-dimensional time-domain signals into two-dimensional time-frequency spectrogram images, which are subsequently input into a pre-trained AlexNet transfer learning model to achieve online identification of the coal rock firmness coefficient grade. In preliminary tests, this method achieved an identification accuracy of 95.58% and a response time of approximately 0.6 s, meeting the requirements for real-time control. The identified result serves as the input variable f for the FNN controller proposed in this paper, enabling the control system to adaptively adjust cutting parameters under unknown operating conditions.

5. Design and validation of the intelligent cutting control system

5.1. Overall system design

5.1.1. System fundamental principles and framework

The system employs a hierarchical control architecture. The primary objective is to ensure structural safety by constraining the cutting arm stress (σ < 125 MPa). Under this safety constraint, the secondary objective is to optimize the SCE (Hw) to improve energy efficiency. The controller's inputs are the key system state variables obtained through real-time sensing and processing, including: the coal-rock hardness coefficient ($f \in [1.5, 3]$), stress ($\sigma \in [80, 130]$ MPa), and specific energy consumption ($H_w \in [4, 13]$ kW·h/m³). The controller outputs are the adjustment values for the drum speed (Δn) and the cutting arm swing speed (Δv). These are synthesized to form the final control commands (ncmd, vcmd) to drive the virtual prototype.

To achieve intelligent, safe, and efficient cutting of the continuous miner under complex coal-rock conditions, a closed-loop control system based on ADAMS and MATLAB/Simulink co-simulation was constructed (Figure 13). The system consists of five core modules:

(1) Controlled Plant (ADAMS Virtual Prototype): This module receives the drum speed command (ncmd) and the cutting arm swing speed command (v_{cmd}) from the controller. It simulates the dynamic behavior of the entire machine, including the flexible cutting arm, and outputs raw physical signals such as stress, loads, and kinematic parameters in real-time.

(2) State Perception and Data Processing Module: This module extracts the key state indicators from the raw signals acquired from ADAMS: the coal-rock hardness coefficient (f), the stress at the critical point of the cutting arm (σ), and the SCE (H_w).

(3) Fuzzy Neural Network (FNN) Controller: Using the state variables (f, σ, H_w) as inputs, this controller first performs qualitative decision-making by simulating expert experience through fuzzy inference. Subsequently, the decision results are nonlinearly optimized via the neural network component, ultimately outputting precise adjustment values for the drum speed and cutting arm swing speed (Δn, Δv).

(4) Control Command Generation Module: This module converts the incremental adjustment commands (Δn, Δv) from the FNN controller into the absolute control commands (n_{cmd}, v_{cmd}) required to drive the ADAMS virtual prototype.

(5) Parallel Safety Protection Module: This is an independent, highest-priority safety protection module. It explicitly overrides the control when the stress exceeds the predefined limit to ensure safety.

The ADAMS virtual prototype operates under the drive of the control commands, and its state is perceived in real-time and fed back to the FNN controller. The controller then generates new optimized commands through intelligent calculation, and this cycle continues. Simultaneously, the parallel safety protection module monitors the system to ensure the stress never exceeds the limit under any circumstances.

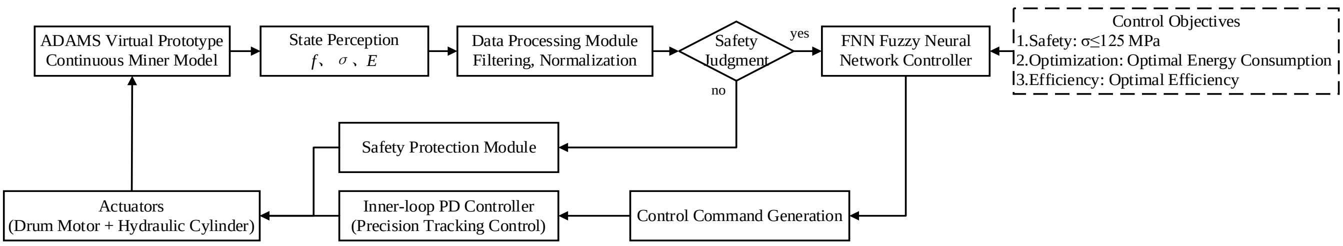

Figure 13. Overall system framework diagram.

5.1.2. Mathematical model of the controlled plant

To facilitate controller design, a surrogate model was established based on simulation data to approximate the input-output relationship of the cutting system. The model takes three inputs-drum speed (n), swing speed (v), and coal-rock hardness coefficient (f)—and outputs two critical indicators: cutting arm stress (σ) and SCE (H_w).

The mapping relationships are defined as:

$$\sigma = f_\sigma(f, n, v, \theta) \tag{5}$$

$$H_W = f_E(f, n, v) \tag{6}$$

where f_σ and f_E are nonlinear mapping functions learned from ADAMS simulation data via response surface methodology (Section 4.2). This surrogate model serves as a computationally efficient replacement for the high-fidelity ADAMS model, enabling rapid internal calculations and gradient solving during FNN controller optimization. The high goodness-of-fit (R^2 = 0.976 for σ, R^2 = 0.983 for H_w) ensures sufficient accuracy for control design.

5.2. Design of the fuzzy neural network controller

5.2.1. Design of the fuzzy controller

The fuzzy controller serves as the core of the intelligent decision-making system, transforming complex expert knowledge and operational experience into computable control logic. The input variables (f, σ, H_w) and output variables (Δn, Δv) were fuzzified. The design of their membership functions and rule base was based on the following principles.

(1) Design of Membership Functions

The membership functions for the input and output variables are designed as shown in Figure 14. Their types (shapes) and parameters are primarily determined based on the characteristics of the variables and the requirements of the control objectives.

Input Variables:

Coal-rock hardness coefficient (f): Its universe of discourse is [1.5, 3]. Triangular membership functions are used, dividing the domain into three fuzzy sets: Low (L), Medium (M), and High (H). This design covers the typical range from soft coal to hard rock, aiming to effectively differentiate between various coal-rock hardness levels.

Cutting arm stress (σ): Its universe of discourse is [80, 130] MPa. To achieve precise perception and rapid response near the safety threshold, a denser division and trapezoidal membership functions with higher overlap are adopted in the high-stress region (>115 MPa). It is also divided into three fuzzy sets: Low (L), Medium (M), and High (H). This ensures that when stress approaches the 125 MPa limit, the "High Stress" state is triggered promptly, enhancing the system's sensitivity for safety response.

SCE (H_w): Its universe of discourse is [4, 13] kW • h/m³. Triangular membership functions are used, dividing the domain into three fuzzy sets: Low (L), Medium (M), and High (H), to characterize the system's energy efficiency level.

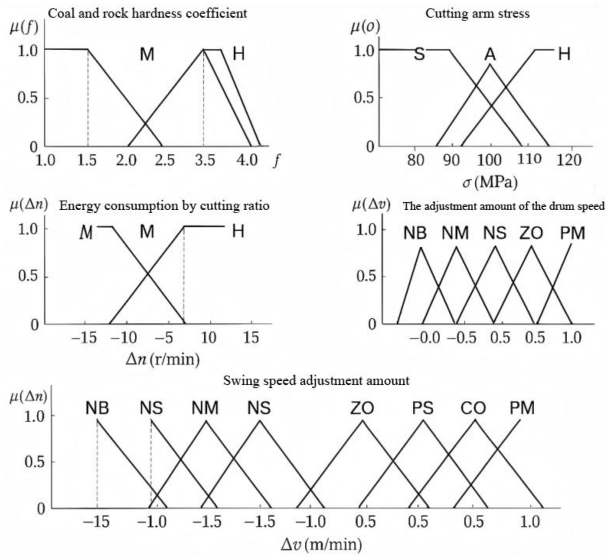

Figure 14. Design of membership functions for input and output variables.

Output Variables:

Rotational speed adjustment (Δn): Its universe of discourse is [-5, +15] r/min. It is divided into six fuzzy sets: Negative Big (NB), Negative Small (NS), Zero (ZO), Positive Small (PS), Positive Medium (PM), and Positive Big (PB). Triangular membership functions are employed to enable fine and smooth speed adjustment.

Swing speed adjustment (Δv): Its universe of discourse is [-2.0, +1.0] m/min. It is divided into six fuzzy sets: Negative Big (NB), Negative Medium (NM), Negative Small (NS), Zero (ZO), Positive Small (PS), and Positive Medium (PM). Given that swing speed has a more direct and sensitive impact on cutting load and stress, its universe is more finely divided with smaller adjustment steps. This prioritizes system stability and safety.

(2) Design of the Fuzzy Rule Base

Based on the operating principles of the continuous miner and the simulation analysis conclusions from Chapter 4, a fuzzy control rule base comprising 27 rules was formulated, as shown in Table 4. These rules simulate the decision-making logic of an experienced operator when faced with different combinations of working conditions.

Table 4. Fuzzy control rule base.

Rule Number	Input Variables			Output Variables		Control Logic Description
	Coal-rock Hardness (*f*)	Cutting Arm Stress (σ, MPa)	SCE (H_w, kW·h/m³)	Rotational Speed Adjustment (Δn, r/min)	Swing Speed Adjustment (Δv, m/min)	
1	L	L	L	NS(-5)	PM(+1.0)	Increase swing speed for higher
2	L	L	M	ZO(0)	PS(+0.5)	Fine-tune for improved
3	L	L	H	PS(+5)	NS(-1.0)	Increase drum speed and
4	L	M	L	NS(-5)	PS(+0.5)	Slightly increase swing speed.
5	L	M	M	ZO(0)	ZO(0)	Maintain current settings.
6	L	M	H	PM(+10)	NS(-1.0)	Optimize parameters.
7	L	H	L	PS(+5)	NM(-1.5)	Prioritize reducing swing
8	L	H	M	PM(+10)	NM(-1.5)	Adjust both parameters.
9	L	H	H	PM(+10)	NB(-2.0)	Enforce aggressive adjustment.
10	M	L	L	NS(-5)	PS(+0.5)	Moderately increase swing
11	M	L	M	ZO(0)	ZO(0)	Maintain settings.
12	M	L	H	PM(+10)	NS(-1.0)	Optimize parameters.
13	M	M	L	ZO(0)	ZO(0)	Optimal point; maintain.
14	M	M	M	PS(+5)	NS(-1.0)	Fine-tune for optimization.
15	M	M	H	PM(+10)	NM(-1.5)	Apply significant adjustment.
16	M	H	L	PM(+10)	NM(-1.5)	Safety first; reduce load.
17	M	H	M	PM(+10)	NB(-2.0)	Strengthen safety measures.
18	M	H	H	PB(+15)	NB(-2.0)	Apply extreme adjustment.
19	H	L	L	PS(+5)	ZO(0)	Apply preventive adjustment.
20	H	L	M	PM(+10)	NS(-1.0)	Apply preemptive adjustment.
21	H	L	H	PM(+10)	NM(-1.5)	Optimize parameters.
22	H	M	L	PM(+10)	NS(-1.0)	Apply preventive
23	H	M	M	PM(+10)	NM(-1.5)	Apply active adjustment.
24	H	M	H	PB(+15)	NM(-1.5)	Apply substantial adjustment.
25	H	H	L	PB(+15)	NB(-2.0)	Prioritize safety strategy.
26	H	H	M	PB(+15)	NB(-2.0)	Apply maximum safety
27	H	H	H	PB(+15)	NB(-2.0)	Apply maximum safety

The core principles guiding the rule design are as follows:

Safety Priority Principle: When the cutting arm stress (σ) is at the "High" (H) level, regardless of other parameters, the control strategy prioritizes stress reduction. This is reflected in Rules 7-9, 16-18, and 25-27, which enforce unloading by significantly reducing the swing speed (Δv set to NB or NM) and, when necessary, increase the rotational speed to enhance rock-breaking capability.

Energy Efficiency Optimization Principle: Within the safe stress range (σ at L or M), the system aims to minimize the SCE (H_w). For example, Rules 1, 4, and 10 allow for a moderate increase in swing speed to boost production when energy consumption is low. Conversely, Rules 3, 6, and 12 optimize the cutting process by "increasing rotational speed and decreasing swing speed" when energy consumption is high, seeking a new efficient operating point.

Condition-Adaptive Principle: The rules adopt differentiated control strategies based on the coal-rock hardness coefficient (*f*). For soft coal (*f* at L), the strategy is relatively aggressive, focusing on efficiency improvement. For hard rock (*f* at H), the strategy becomes more conservative, emphasizing preventive protection and maintaining stability.

5.2.2. Design of the neural network optimizer

To overcome the limitations of the fuzzy controller in terms of control precision and to further enhance the system's adaptive capability to complex nonlinear working conditions, a neural network optimizer was designed to precisely refine the control decisions. This network works in synergy with the fuzzy controller, together forming the intelligent decision-making core of the Fuzzy Neural Network (FNN).

(1) Network Structure and Training Algorithm

A single-hidden-layer feedforward (Backpropagation, BP) neural network was employed. Its specific architecture is illustrated in Figure 15.

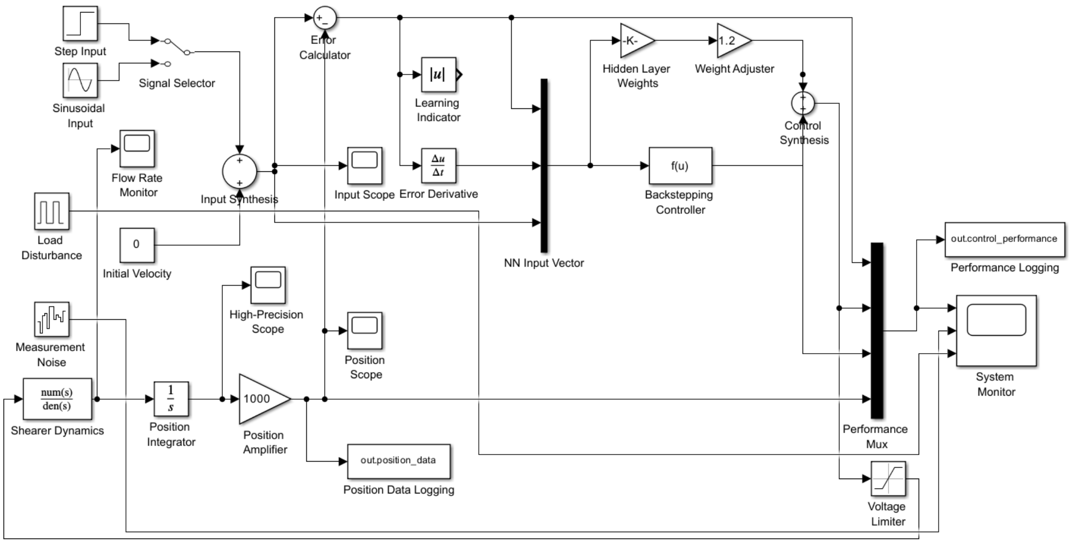

Figure 15. Neural network controller module.

Network Topology: The architecture is 3-8-2, comprising 3 input neurons, 8 hidden layer neurons, and 2 output neurons.

Input and Output: The network takes the three real-time system state parameters (f, σ, H_w) as its inputs and directly outputs the optimized adjustment values for the drum rotational speed and the cutting arm swing speed (Δn, Δv).

Activation Function: A Sigmoid activation function is employed for the hidden layer neurons. Its expression is:

$$\sigma(x) = \frac{1}{1+e^{-x}} \tag{7}$$

This function provides a smooth nonlinear mapping, making it suitable for this control system.

Training Algorithm: The network training utilizes the Levenberg-Marquardt (L-M) algorithm. This algorithm combines the advantages of the gradient descent and Gauss-Newton methods, featuring fast convergence and high accuracy. Its weight update rule is:

$$\Delta \mathrm{w} = -[J^T J + \mu I]^{-1} J^T e \tag{8}$$

where: J is the Jacobian matrix; e is the error vector; and μ is the damping parameter.

5.2.3. Training data and process

(1) Training Dataset Construction

A total of 1,240 datasets were used for neural network training, combining 240 original simulation datasets (from ADAMS-MATLAB co-simulation with $f \in [1.5,3]$, $n \in [31,71]$ r/min, $v \in [3,7]$ m/min) and 1,000 response surface-augmented datasets generated via Latin Hypercube Sampling using the high-precision model (R^2=0.987) from Section 4.2, with energy consumption from Section 2.4.3. This hybrid “simulation + augmentation” strategy preserves physical authenticity while enhancing generalization across the parameter space.

(2) Network Structure and Training

Network Topology: A three-layer feedforward BP neural network with a 3-8-2 structure was adopted, consisting of 3 input neurons (f, σ, H_w), 8 hidden layer neurons, and 2 output neurons (Δn, Δv). The Sigmoid activation function was employed in the hidden layer, and the network was trained using the Levenberg-Marquardt (L-M) algorithm.

Determination of Hidden Layer Node Number: The number of hidden layer nodes was determined to be 8 through comparative experiments. Experiments showed that fewer than 8 nodes led to underfitting, failing to adequately capture the complex relationships within the data, while more than 8 nodes tended to cause overfitting and a decline in generalization capability. The 8-node structure achieved the best balance between model accuracy and generalization ability.

Dataset Partitioning: To rigorously evaluate the model's performance, the total of 1,240 samples were randomly partitioned into a training set and a test set at a 4:1 ratio. Specifically, the training set comprised 992 samples, and the test set comprised 248 samples.

Training Objective: The training process aims to minimize the Mean Squared Error (MSE). The loss function is defined as:

$$MSE = \frac{1}{N_{samples}} \cdot \sum_{j=1}^{N_{samples}} \sum_{k=1}^{N_{outputs}} (d_{jk} - y_{jk})^2 \tag{9}$$

(3) Training Results and Performance Validation

The network's training convergence process and prediction performance are illustrated in Figure 16 and Figure 17, respectively.

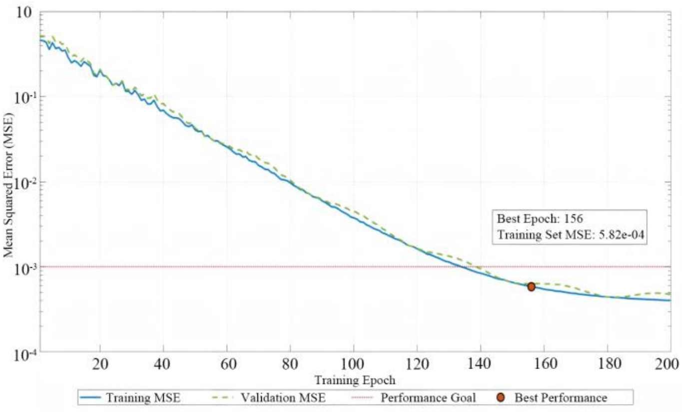

Figure 16. Convergence process of neural network training.

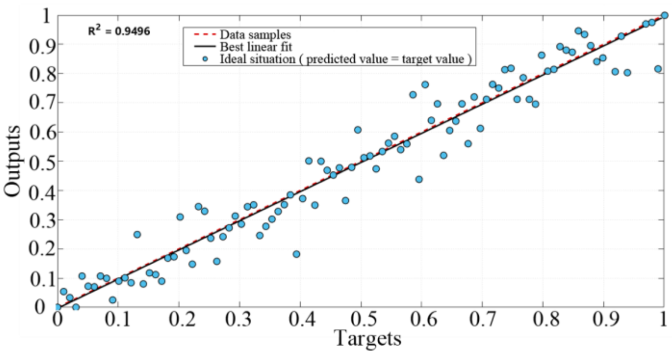

Figure 17. Validation of the neural network model's prediction performance.

Convergence: As shown in Figure 16, the training process converged rapidly. The Mean Squared Error (MSE) decreased to 5.82×10^{-4} after 156 epochs, meeting the preset accuracy requirement. This demonstrates the effectiveness of the L-M algorithm for the problem at hand.

Generalization Capability: The validation results on the 248-set independent test set (Figure 17) demonstrate that the network's predicted values are in excellent agreement with the true simulation values. The scatter points are tightly distributed around the y=x diagonal line, with a coefficient of determination $R^2 = 0.962$ and a root mean square error (RMSE) of 0.28 MPa. This strongly confirms that the trained neural network model possesses outstanding prediction accuracy and robust generalization capability, making it reliable for embedding into the control system as an intelligent optimization unit.

Generalization Capability Validation under Boundary Conditions: To evaluate the prediction reliability of the neural network under extreme operating conditions, a boundary condition characterized by high hardness (f = 3), high swing speed (v = 7 m/min), and low rotational speed (n = 31 r/min) was selected for dedicated validation. The state parameters under this condition were input into the trained neural network, yielding the control parameter adjustments (Δn = +15 r/min, Δv = -2.0 m/min). These adjustments were then substituted into the ADAMS model for closed-loop simulation. The results show that the peak stress predicted by the neural network is 124.9 MPa, while the ADAMS simulation result is 124.7 MPa, corresponding to a relative error of only 0.16%. This verifies the prediction reliability of the model under boundary conditions.

5.2.4. Design of the safety protection mechanism

A parallel safety protection mechanism, independent of the main control logic and possessing the highest priority, was designed. Its logic is illustrated in Figure 18. This mechanism employs a three-level protection strategy:

Level 1: Warning (σ > 115 MPa): The system issues an alarm signal and restricts any further increase in the cutting arm swing speed.

Level 2: Emergency (σ > 120 MPa): The system enforces a set of conservative cutting parameters.

Level 3: Critical (σ > 125 MPa): The system forcibly reduces the cutting arm swing speed to a preset minimum safe value (vmin), while simultaneously increasing the drum speed to a preset maximum value (nmax), to achieve forced unloading.

This module is implemented via a logic selector. When the stress exceeds the limit, it overrides the FNN commands with higher priority, ensuring that the cutting arm stress never surpasses the material's allowable stress under any working condition, thereby providing reliable safety protection for the system.

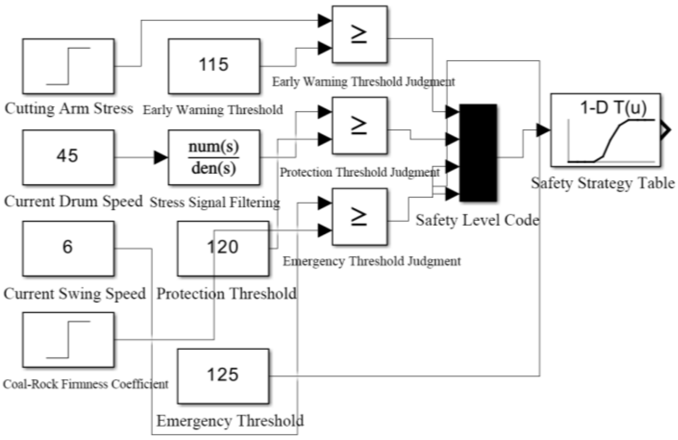

Figure 18. Safety protection module.

5.2.5. Inner-loop controller and parameter tuning

Given the dynamic response delays of the actuators and the variable load conditions, a high-response inner-loop PI control circuit is incorporated into the system. This circuit ensures the fast and precise tracking of the rotational and swing speed commands generated by the upper-layer intelligent decision-making module. It is responsible for receiving the target commands from the FNN output and driving the actuators (e.g., motors, hydraulic cylinders) within the ADAMS virtual prototype for accurate tracking.

(1) Inner-loop Controller Structure

The inner-loop controller adopts a classical PI (Proportional-Integral) control structure, independently controlling the drum speed (n) and the cutting arm swing speed (v). The control laws are as follows:

For drum speed control:

$$u_n = k_{p,n}e_n + k_{i,n}\int e_n dt \tag{10}$$

where: $e_n = n_{target} - n_{actual}$, is the speed tracking error; k(p,n) and k(i,n) are the proportional and integral gains, respectively.

For cutting arm swing speed control:

$$u_v = k_{p,v}e_v + k_{t,v}\int e_v dt \tag{11}$$

where: $e_v = v_{target} - v_{actual}$, is the swing speed tracking error; k(p,v) and k(i,v) are the proportional and integral gains, respectively.

(2) Controller Parameter Tuning and System Configuration

The parameters of the inner-loop PI controllers were initially tuned using the classical Ziegler-Nichols method and finalized through extensive simulations. The final determined parameters are:

Drum Speed Loop: Proportional gain k (p,n) = 0.85; Integral gain k (i,n) = 0.35.

Swing Speed Loop: Proportional gain k (p,v) = 0.75; Integral gain k (i,v) = 0.28.

To ensure the real-time performance and stability of the co-simulation, the control system's sampling period is set to 20 ms. This period satisfies the real-time requirements for data exchange between ADAMS and Simulink while maintaining control accuracy.

Finally, the cutting system model was exported via ADAMS/Controls as an S-Function and integrated into Simulink, where it was combined with all functional modules—including the FNN controller, inner-loop PI controllers, safety protection module, and ADAMS interface—to construct a complete closed-loop simulation system (as shown in Figure 19). This model clearly illustrates the data flow connections between modules, forming a comprehensive control architecture that spans from intelligent decision-making to low-level execution.

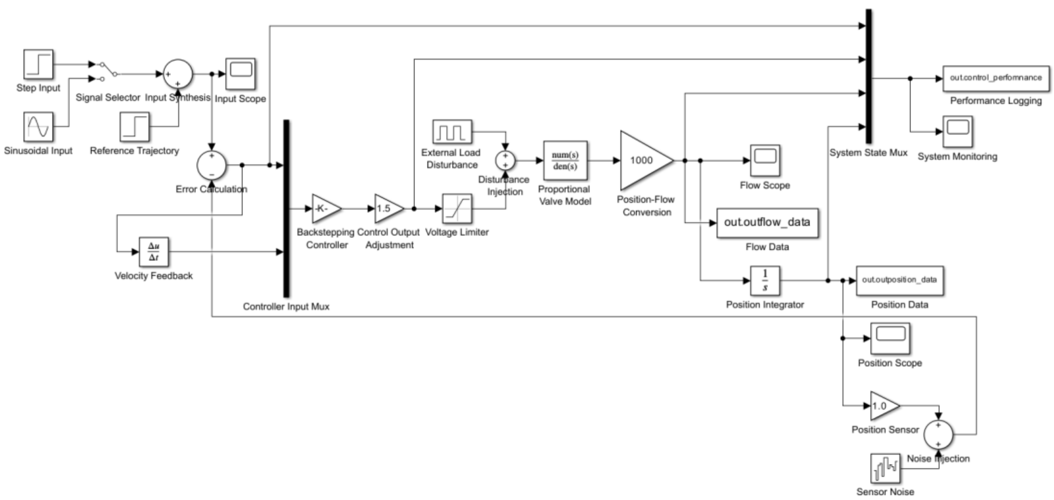

Figure 19. Simulink model.

5.3. Performance analysis

5.3.1. Verification of adaptive control performance

To verify the adaptive regulation capability of the FNN controller under unknown changes in operating conditions, a simulation scenario involving bidirectional sudden changes in hardness was designed. The controller made autonomous decisions solely based on real-time detected cutting arm stress σ and specific energy consumption H_w, without any pre-input information regarding hardness changes.

The simulation operating conditions were set as follows: The system initially operated under soft coal conditions ($f = 1.5$). To simulate common sudden hardness changes encountered in actual cutting, the hardness unexpectedly jumped to $f = 2.5$ at $t = 20$ s, further jumped to $f = 3.0$ at $t = 35$ s, and then dropped back to $f = 1.5$ at $t = 50$ s. Throughout the entire process, the controller needed to autonomously perceive the changes in operating conditions and make corresponding adjustments.

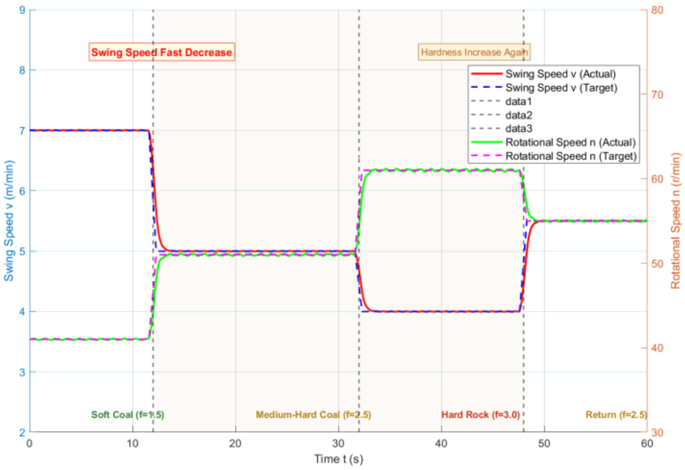

Figure 20. FNN controller adaptive regulation under variable hardness conditions.

The simulation results are shown in Figure 20. From the figure, it can be observed:

(1) Response to hardness increase: When the hardness suddenly increased at $t = 20$ s and $t = 35$ s, the controller detected a rapid rise in stress and immediately made a coordinated decision to "decrease the swing speed and increase the rotation speed." The swing speed autonomously decreased from 7 m/min to 5 m/min and then to 4 m/min, respectively, while the rotation speed autonomously increased from 41 r/min to 51 r/min and then to 61 r/min, respectively. This indicates that the controller can autonomously determine the deterioration of operating conditions based on stress feedback and take protective measures.

(2) Response to hardness decrease: When the hardness dropped back to $f = 1.5$ at $t = 50$ s, the controller detected a decrease in stress and autonomously increased the swing speed from 4 m/min back to 6.5 m/min, while reducing the rotation speed from 61 r/min back to 43 r/min. This verifies that the controller possesses bidirectional adaptive capability, enabling it to automatically resume efficient cutting conditions after the operating environment improves.

(3) Safety constraint satisfaction: Throughout the entire dynamic regulation process, the peak stress of the cutting arm was always strictly maintained below the safety threshold of 125 MPa, verifying the safety assurance capability of the FNN controller under unknown disturbances.

5.3.2. Ablation experiment

To verify the necessity of combining 'fuzzy control' with 'BP neural network' in the FNN controller, an ablation experiment was designed. Under the same hard rock impact condition (f stepped from 1.5 to 3.0 at $t = 20$ s), the performance of a pure fuzzy controller, a pure BP neural network controller, and the proposed FNN controller was compared. The results are shown in Table 5, and the stress response comparison curves of the ablation experiment are presented in Figure 21.

Table 5. Ablation experiment results.

Performance metrics	Pure fuzzy control	Pure BP neural network	Proposed FNN
Peak stress (MPa)	125.8	126.2	124.9
Overshoot (%)	5.2	4.8	3.9
Settling time (s)	1.4	1.1	0.8
Steady-state error (MPa)	≈0.4	≈0.3	<0.2
Safety constraint violation (≤125 MPa)	Yes	Yes	No
Average specific	8.1	8.0	7.8

Result analysis: The pure fuzzy controller is capable of making reasonable qualitative decisions based on expert rules, such as promptly reducing the swing speed when stress becomes too high. However, due to the limitations of discretized quantization of membership functions and fixed rule weights, it exhibits a relatively large steady-state error (approximately 0.4 MPa). Moreover, at the moment of sudden hardness change, the peak stress reaches 125.8 MPa, slightly exceeding the safety limit. This indicates that although pure fuzzy control offers good interpretability and safety-oriented design, its control accuracy is limited.

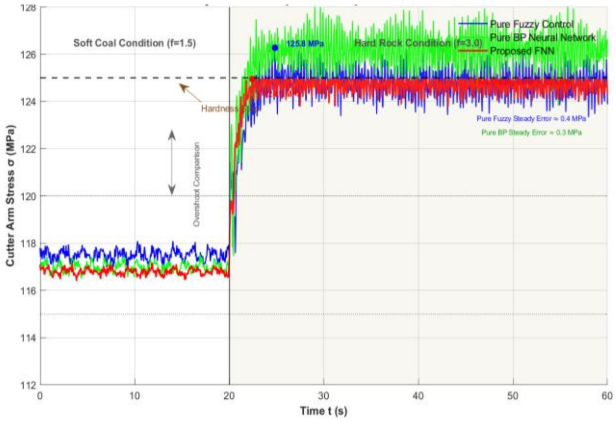

Figure 21. Ablation experiment stress response comparison curves.

The pure BP neural network controller, leveraging its powerful nonlinear fitting capability, outperforms pure fuzzy control in terms of settling time (1.1 s) and steady-state error (approximately 0.3 MPa). However, since the training objective of the neural network is to minimize the global mean square error (MSE) rather than explicitly satisfying the safety constraint ($\sigma \leq 125$ MPa), its output may violate the safety limit under extreme operating conditions (peak stress reaching 126.2 MPa). Furthermore, pure neural network control lacks interpretability and makes it difficult to embed expert prior knowledge.

The proposed FNN controller successfully integrates the advantages of both approaches: the fuzzy control part provides rule-based qualitative decision-making and safety prior constraints, while the neural network part performs refined nonlinear optimization on this basis. Experimental results show that the FNN achieves the best overall performance-the shortest settling time (0.8 s), the smallest overshoot (3.9%), the lowest steady-state error (<0.2 MPa), and the peak stress strictly controlled at 124.9 MPa, satisfying the safety constraint throughout the entire process. Additionally, thanks to intelligent collaborative optimization, the average specific energy consumption is also minimized (7.8 kW • h/m^3).

5.3.3. Robustness analysis of the control system

To evaluate the performance of the designed Fuzzy Neural Network (FNN) controller in the presence of model mismatch and parameter uncertainties, a quantitative robustness analysis was conducted. The analysis method involved artificially applying different levels of random perturbations to the FNN controller's key internal parameters (including the centers of the membership functions, neural network connection weights, etc.) and performing closed-loop simulation tests under standard hard rock conditions (f = 3.0).

As shown in Figure 22, the stress response of the cutting arm of the system under ±10%, ±30%, and ±50% perturbations in the controller parameters is compared with the response under the nominal (unperturbed) condition. The results demonstrate that:

Performance under Mild to Moderate Perturbations: When parameter variations are within ±30%, the stress response curve of the system shows only minor deviations from the ideal curve. Although the peak stress increases slightly, it remains strictly below the safe allowable stress limit of 124.9 MPa. No significant degradation in system stability or dynamic response speed is observed.

Stability under Severe Perturbations: Even with parameter perturbations as high as ±50%, although the control system exhibits performance degradation-manifested as increased overshoot and longer settling time-the closed-loop system remains stable without divergence or sustained oscillation. Most critically, the peak stress never exceeds the safety threshold, demonstrating the system's fundamental safety assurance capability.

This robustness analysis fully verifies the insensitivity of the proposed FNN intelligent control system to internal parameter perturbations. Even when confronted with significant model uncertainties, the system maintains stable and safe basic control functions. This characteristic is essential for ensuring the reliable application of the control system in real and variable industrial environments.

5.3.4. Fatigue life assessment

Based on the stress time-history at Node 198, a preliminary fatigue life assessment was performed using the ADAMS/Durability module (rainflow counting and Miner's linear damage rule). Under open-loop control, the estimated fatigue life is approximately 2.3×106 cycles; with the proposed FNN controller, it increases to approximately 4.1×106 cycles (a 78% improvement), indicating that reduced stress fluctuations effectively lower the risk of crack initiation and fracture.

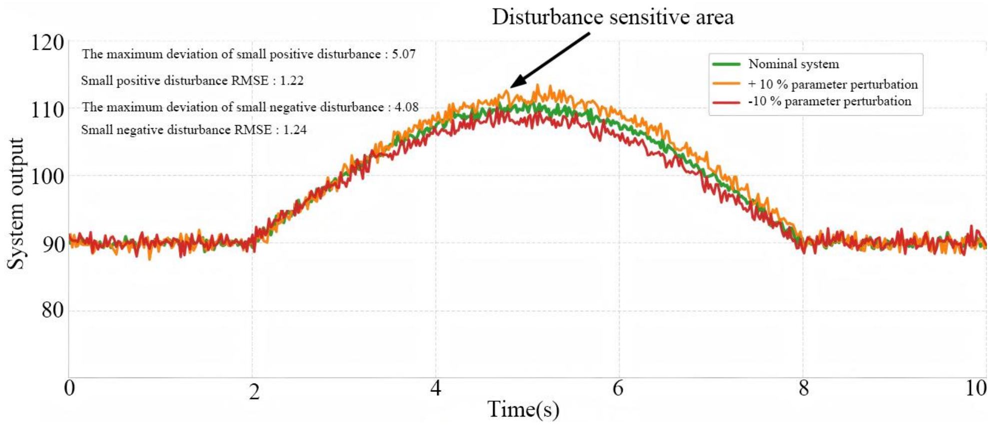

(a) 10% parameter perturbation

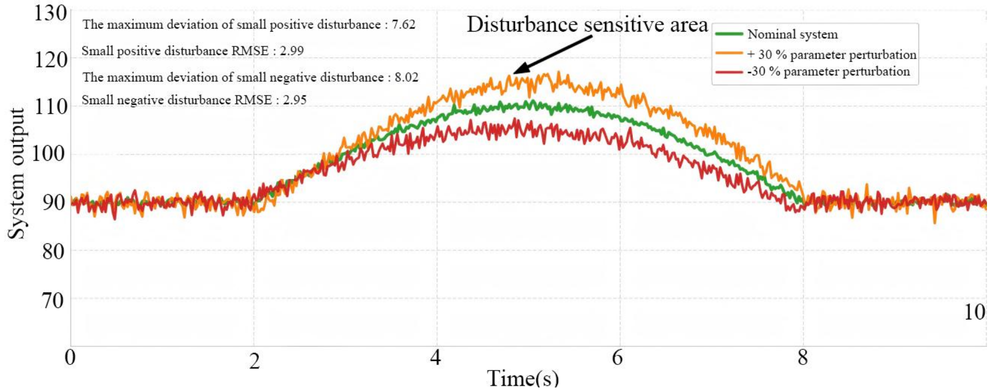

(b) 30% parameter perturbation

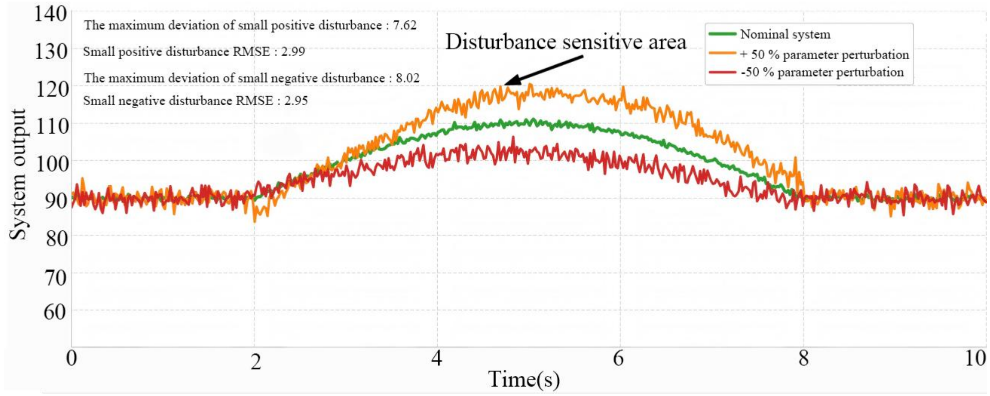

(c) 50% parameter perturbation

Figure 22. Robustness analysis of the control system under parameter perturbations.

6. Experimental verification

6.1. Test bench construction

A continuous miner coal-rock cutting test bench was constructed according to the similarity theory, taking the left cutting drum as an example for assembly. As shown in Figure 23, the test bench consists of an artificial coal wall, the left drum of the continuous miner cutting unit, a power system, and a data acquisition system. Based on a certain working face of the Zhangjiamao coal mine, coal wall physical models were fabricated by mixing sand, cement, gypsum, and water in different proportions to ensure consistency in performance between the similar coal wall and actual coal rock. To collect drum vibration signals, a Bluetooth wireless acceleration sensor was installed at the rear end of the drum. Before testing, the cutting unit was moved back and forth on the guide rails several times to check the operating status of all systems. After confirming proper functionality, the push cylinder was used to advance the spiral drum toward the coal wall until the drum picks made contact, and the acceleration data collected during the tests were transmitted wirelessly to a computer for display, storage, and analysis.

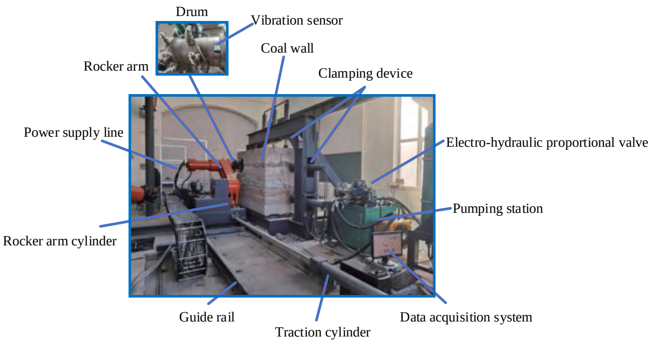

Figure 23. Continuous miner cutting test bench.

6.2. Vibration acceleration

The accuracy of the vibration acceleration of the drum obtained through ADAMS virtual simulation was verified using the test platform. The simulation and experimental curves of the vibration acceleration in the cutting resistance direction under stable cutting conditions of the left drum were extracted. The results are shown in Figure 24.

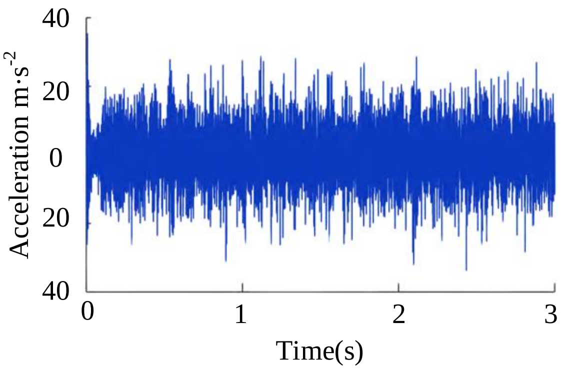

(a) simulation

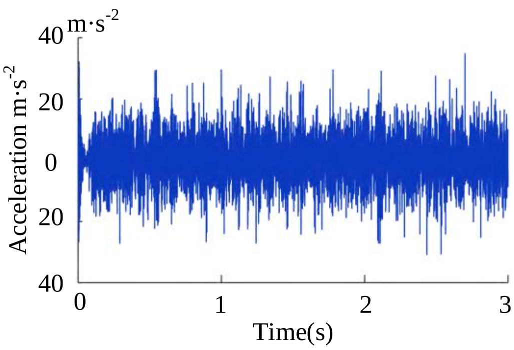

(b) experiment

Figure 24. Comparison of drum vibration acceleration under different conditions.

As shown in Figure 24, the vibration characteristic waveforms from the experiment and the virtual simulation exhibit high similarity, with fluctuations approximately in the range of -19,300 mm/s^2 to 19,000 mm/s^2. Calculation based on the exported sampling point data indicates that the maximum relative error of the vibration acceleration characteristic values between the two is 4.92%, which falls within a reasonable margin. In summary, these results confirm the feasibility and accuracy of the ADAMS virtual simulation method.

6.3. Experimental scheme for variable-hardness cutting

To verify the adaptive regulation performance of the FNN controller during actual cutting processes, variable-hardness coal-rock cutting experiments were conducted on the cutting test bench. The coal-rock specimens were prepared using a segmented pouring method, with consistency coefficients *f* of 1.5, 2.0, 2.5, and 3.0, respectively. Each segment had a length of 0.5 m, with a total length of 2.0 m. The experiments were divided into two working conditions: hardness increasing (1.5-3.0) and hardness decreasing (3.0-1.5), to verify the response capability of the FNN controller under different variation trends.

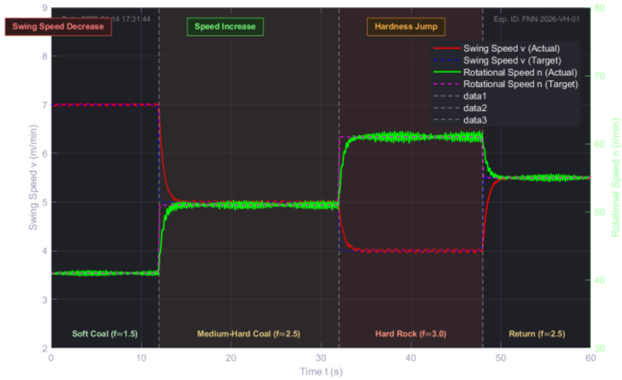

Figure 25. Experimental regulation of FNN controller under different f values.

Figure 25 illustrates the regulation process of the FNN controller under the hardness-increasing working condition. It can be observed from the figure that the hardness identification module based on drum vibration signals can identify hardness changes in real time, with a lag time of approximately 0.5 s. When the hardness increased from 1.5 to 2.0, the swing speed decreased from 6.8 m/min to 6.0 m/min, while the rotational speed increased from 52 r/min to 58 r/min. When the hardness further increased to 3.0, the swing speed further decreased to 4.2 m/min, and the rotational speed increased to 68 r/min. The regulation process was smooth without severe oscillations. After a sudden hardness change, the controller completed parameter adjustment within approximately 0.8 s, which is consistent with the simulation result (0.8 s).

6.4. Comparison and verification between simulation and experiment

Table 6 compares the key performance indicators of the FNN controller in simulation and experiment, taking f=3 as an example. The relative errors of all indicators are within 3%, verifying the accuracy of the simulation model and the engineering feasibility of the FNN controller.

Table 6. Comparison between simulation and experiment.

Performance Indicators	Simulation Value	Experimental Value	Relative Error
Stable swing speed (m/min)	4.2	4.15	1.2%
Stable rotational speed (r/min)	68	67.5	0.7%
Adjustment time (s)	0.8	0.82	2.5%

Direct dynamic stress measurement remains challenging with current test bench configuration; therefore, this study indirectly validates the simulation model and control strategy through a combined "vibration response + control parameter adjustment" approach, demonstrating the feasibility of performance verification under constrained experimental conditions.

7. Conclusion

(1) Dynamic simulation and strength risk identification: A rigid-flexible coupled virtual prototype was successfully constructed. Dynamic simulation revealed that under baseline conditions (f = 3, n = 41 r/min, v = 7 m/min), the hydraulic cylinder connection point of the cutting arm is a critical high-stress location, with a peak stress of 128.93 MPa exceeding the allowable limit (125 MPa). Single-factor and response surface analyses quantified the coupled effects of drum speed, swing speed, and coal-rock hardness on peak stress and SCE, with local sensitivity identifying swing speed as the most influential factor on stress (sensitivity 2.80) and drum speed on SCE (sensitivity 4.10).

(2) Online identification and FNN intelligent control: A cutting vibration response-based method using an AlexNet transfer learning model was proposed for online identification of the coal-rock hardness coefficient, achieving 95.58% accuracy with a response time of 0.6 s. Based on this, an FNN controller with a three-level parallel safety protection module (warning at 115 MPa, emergency at 120 MPa, critical at 125 MPa) was designed. Co-simulation and ablation experiments demonstrate that the FNN controller outperforms pure fuzzy and pure BP neural network counterparts, adaptively adjusting parameters under sudden hardness changes while strictly confining peak stress within the safety limit.

(3) Robustness and energy efficiency: Robustness analysis confirms stable operation even under ±50% perturbations to internal controller parameters, demonstrating strong insensitivity to model uncertainties. Under safety constraints, the proposed strategy reduces average SCE by 9.3% under variable load conditions.

(4) Experimental validation: A physical cutting test bench was constructed based on similarity theory. Comparison of drum vibration characteristics between simulation and experiment shows a maximum relative error of 4.92%, validating the simulation accuracy. Variable-hardness cutting experiments further confirm the FNN controller's adaptive regulation performance under both hardness-increasing and hardness-decreasing conditions, with adjustment time of approximately 0.8 s, consistent with simulation results.

References

1. Li W T. Research on cutting characteristics of shearer under different coal-rock mechanical properties. *Taiyuan University of Technology* 2023. https://doi.org/10.27352/d.cnki.gylgu.2023.001352.
2. Wang G F, Liu F, Meng X J, Fan J D, Wu Q Y, Ren H W, Zhang K. Research and practice on intelligent coal mine construction (primary stage). *Coal Science and Technology* 2019; 47(8): 1-36. https://doi.org/10.13199/j.cnki.cst.2019.08.001.
3. Li R Z. Reinforced design of the cutting unit of MG500/1220-WD shearer. *Coal Mine Machinery* 2011; 32(6): 22-23. https://doi.org/10.13436/j.mkjx.2011.06.099.

4. Zhang X, Liu H J, Guo S L, Zhang L M. Simulation analysis of fatigue life of planetary carrier in shearer cutting unit. *Mining & Processing Equipment* 2013; 41(6): 18-21. https://doi.org/10.16816/j.cnki.ksjx.2013.06.006.
5. Lei X Q, Yang Z J, Wang Y L. Reliability study of shearer cutting unit based on rigid-flexible coupling. *Mining & Processing Equipment* 2014; 42(7): 25-29. https://doi.org/10.16816/j.cnki.ksjx.2014.07.007.
6. Zhao L J, Yang Y, Li M H. Fatigue analysis of gears in shearer cutting unit transmission system based on ANSYS. *Journal of Mechanical Transmission* 2014; 38(7): 135-137. https://doi.org/10.16578/j.issn.1004.2539.2014.07.002.
7. Liu S H. Reliability analysis of shearer cutting unit based on computer simulation technology. *Coal Technology* 2014; 33(12): 291-292. https://doi.org/10.13301/j.cnki.ct.2014.12.102.
8. Liu X. Finite element analysis of torque shaft in shearer cutting unit based on ANSYS. *Coal Mine Machinery* 2020; 41(4): 178-180. https://doi.org/10.13436/j.mkjx.202004060.
9. Wang G. Strength analysis of shearer pin shaft based on co-simulation of ADAMS and ANSYS. *Coal Mine Machinery* 2020; 41(1): 181-183. https://doi.org/10.13436/j.mkjx.202001060.
10. Liu X N, Zhao L J, Huang K, Luo G H. Reliability analysis of key components in shearer cutting unit based on stress-strength interference theory. *Journal of China Coal Society* 2019; 44(3): 965-973. https://doi.org/10.13225/j.cnki.jccs.2018.0505.
11. Liao J B, Li X B, Wang S F, Du K. Effects of cut depth and cut spacing on a conical pick in rock cutting. *Rock and Soil Mechanics* 2023; 44(4): 1009-1021. https://doi.org/10.16285/j.rsm.2022.1667.
12. Ji M T. Influence of pick installation angle on drum performance of shearer and its optimization. *Energy and Environmental Protection* 2023; 45(7): 244-249. https://doi.org/10.19389/j.cnki.1003-0506.2023.07.037.
13. Zhang H Q, Han Z G, Ma C B, et al. Multi-objective optimization of roadheader cutting performance under different working conditions. *Coal Engineering* 2023; 55(9): 103-107.
14. Chi N. Study on the influence of cutting parameters on specific cutting energy consumption of shearer. *Mechanical Management and Development* 2022; 37(8): 125-127. https://doi.org/10.16525/j.cnki.cn14-1134/th.2022.08.054.
15. Wu Q. Research on drum structure optimization of shearer based on discrete element simulation. *Mechanical Management and Development* 2022; 37(10): 52-54. https://doi.org/10.16525/j.cnki.cn14-1134/th.2022.10.023.
16. Świder J, Jasiulek D. Use of a virtual prototyping in construction of a mining machine's control system. *Journal of Achievements in Materials and Manufacturing Engineering* 2009; 36(2): 160-167.
17. Yan L C. Self-adaptive control on hydraulic system of excavators by an improved particle swarm algorithm. *Chinese Hydraulics & Pneumatics* 2012; (8): 105-108.
18. Zhao L J, Li M. Simulation of fuzzy PID control for automatic height adjustment system of shearer. *Journal of Liaoning Technical University (Natural Science Edition)* 2016; 35(10): 1075-1080.
19. Chen J G, Liu C S, Fan J H, Zhang Y J, Wan F. Modeling and simulation of shearer drum height adjustment system. *Industry and Mine Automation* 2017; 43(10): 78-82. https://doi.org/10.13272/j.issn.1671-251x.2017.10.016.
20. Wang H, Zhao G C, Song Y N, Jin X. Trajectory tracking fuzzy PID control for shearer height adjustment process. *Journal of Electronic Measurement and Instrumentation* 2018; 32(8): 164-171. https://doi.org/10.13382/j.jemi.2018.08.023.
21. Mao J, Guo H, Chen H Y. Novel firefly algorithm and its application in PID control of shearer automatic height adjustment. *Journal of Machine Design* 2019; 36(8): 55-60. https://doi.org/10.13841/j.cnki.jxsj.2019.08.009.
22. Liu L T, Dong S T. Adaptive speed control of shearer cutting based on BP neural network. *Coal Mine Machinery* 2020; 41(8): 197-199. https://doi.org/10.13436/j.mkjx.202008064.
23. Guo D, Li J H, Jiang S H, Li X, Chen Z Y. Intelligent assistant driving method for tunnel boring machine based on big data. *Acta Geotechnica* 2022; 17(4): 1019-1030.
24. Zhao L J, Wang Y D, Zhang M C, Jin X, Liu H M. Adaptive cutting control strategy of shearer under complex coal seam conditions. *Journal of China Coal Society* 2022; 47(1): 541-563. https://doi.org/10.13225/j.cnki.jccs.yg21.1862.
25. Liu C S, Liu Y T, Liu R H, Bai Y F, Li D G, Shen J X. Correlation load characteristic model between shearer cutting state and coal-rock recognition. *Journal of China Coal Society* 2022; 47(1): 527-540. https://doi.org/10.13225/j.cnki.jccs.YG21.1792.
26. Cai A J, Liu J Q, Liu Y D, Ren Z G. Research on autonomous height adjustment strategy of shearer based on implicit digital twin. *Mining*

Research and Development 2022; 42(11): 188-194. https://doi.org/10.13827/j.cnki.kyyk.2022.11.004.

27. Zheng C, Li D N, Feng Y H. Intelligent shearer cutting control based on process driven technology. *Industry and Mine Automation* 2024; 50(5): 23-27. https://doi.org/10.13272/j.issn.1671-251x.2023090017.
28. Liu S Y, Cheng C, Wu H Z, Cui Y M, Meng D Y, Si L. Research on intelligent height adjustment control method of shearer based on coal-rock interface recognition. *Coal Science and Technology* 2024; 52(S2): 186-200. https://doi.org/10.13199/j.cnki.cst.2022-0004.
29. Zhang Y P. Study on the influence of kinematic parameters and structural parameters of continuous miner drum on cutting performance. *Liaoning Technical University*; 2024. https://doi.org/10.27210/d.cnki.glnju.2024.000914.
30. Wang Y D. Research on adaptive cutting control of shearer based on CPS concept. *Liaoning Technical University*; 2022. https://doi.org/10.27210/d.cnki.glnju.2022.000871.